

Exploring and enhancing the accuracy of interior-scaled Perdew-Zunger self-interaction correction

Puskar Bhattarai,^{1, a)} Biswajit Santra,¹ Kamal Wagle,¹ Yoh Yamamoto,² Rajendra R. Zope,² Adrienn Ruzsinszky,¹ Koblar A. Jackson,³ and John P. Perdew^{1, 4}

¹⁾ *Department of Physics, Temple University, Philadelphia, PA-19122*

²⁾ *Department of Physics, University of Texas at El Paso, El Paso, Texas 79968, USA*

³⁾ *Department of Physics and Science of Advanced Materials, Central Michigan University, Mount Pleasant, Michigan 48859, USA*

⁴⁾ *Department of Chemistry, Temple University, Philadelphia, PA-19122*

(Dated: 11 January 2021)

The Perdew-Zunger self-interaction correction (PZ-SIC) improves the performance of density functional approximations (DFAs) for the properties that involve significant self-interaction error (SIE), as in stretched bond situations, but overcorrects for equilibrium properties where SIE is insignificant. This overcorrection is often reduced by LSIC, local scaling of the PZ-SIC to the local spin density approximation (LSDA). Here we propose a new scaling factor to use in an LSIC-like approach that satisfies an additional important constraint: the correct coefficient of atomic number Z in the asymptotic expansion of the exchange-correlation (xc) energy for atoms. LSIC and LSIC+ are scaled by functions of the iso-orbital indicator z_σ , which distinguishes one-electron regions from many-electron regions. LSIC+ applied to LSDA works better for many equilibrium properties than LSDA-LSIC and the Perdew, Burke, and Ernzerhof (PBE) generalized gradient approximation (GGA), and almost as well as the strongly constrained and appropriately normed (SCAN) meta-GGA. LSDA-LSIC and LSDA-LSIC+, however, both fail to predict interaction energies involving weaker bonds, in sharp contrast to their earlier successes. It is found that more than one set of localized SIC orbitals can yield a nearly degenerate energetic description of the same multiple covalent bond, suggesting that a consistent chemical interpretation of the localized orbitals requires a new way to choose their Fermi orbital descriptors. To make a locally scaled-down SIC to functionals beyond LSDA requires a gauge transformation of the functional's energy density. The resulting SCAN-sdSIC, evaluated on SCAN-SIC total and localized orbital densities, leads to an acceptable description of many equilibrium properties including the dissociation energies of weak bonds.

I. Introduction

Kohn-Sham density functional theory (KS-DFT)¹ is a computationally efficient approach to calculate the ground state energy and density of many-electron systems. It is widely used to predict various properties of atoms, molecules and solids, because of its computational efficiency in comparison with many-electron wavefunction calculations. The accuracy of KS-DFT for ground state calculations depends upon the approximation for the exchange-correlation energy (E_{xc}) of the system. Jacob's ladder² is often used to classify the approximate density functionals, where higher rungs incorporate additional ingredients that increase both accuracy and computational cost. E_{xc} is often approximated as

$$E_{xc}[n_\uparrow, n_\downarrow] = \int d^3r n \epsilon_{xc}(n_\uparrow, n_\downarrow, \nabla n_\uparrow, \nabla n_\downarrow, \tau_\uparrow, \tau_\downarrow), \quad (1)$$

where

$$n(\mathbf{r}) = n_\uparrow(\mathbf{r}) + n_\downarrow(\mathbf{r}) \quad (2)$$

is the total density and

$$\tau_\sigma(\mathbf{r}) = \sum_i^{occup} \frac{1}{2} |\nabla \psi_{i\sigma}(\mathbf{r})|^2 \quad (3)$$

is the positive kinetic energy density for the occupied orbitals $\psi_{i\sigma}$. The first three rungs include the local spin density approximation (LSDA), generalized gradient approximation (GGA) and meta-GGA. LSDA takes the local electron density as its sole ingredient. GGAs take the gradient of electron density ∇n_σ as an additional ingredient, and meta-GGAs take τ_σ as well. Semi-local non-empirical approximate functionals of higher rungs are often constructed by satisfying more exact constraints and norms than the lower rungs.³ For instance, the PBE⁴ GGA satisfies 11 known exact constraints and the SCAN³ meta-GGA satisfies 17 known exact constraints. The most common norm is the uniform electron gas,⁵ for which almost all the functionals are exact by construction.

All semi-local DFAs suffer from self-interaction error (SIE)⁶ due to the imperfect cancellation of the self-Hartree energy U by the self-exchange-correlation energy E_{xc} of a single fully occupied orbital. The Perdew-Zunger self-interaction correction (PZ-SIC)⁶ removes one-electron SIE by subtracting it on an orbital-by-orbital basis. Hence, the corrected E_{xc} can be written

^{a)} Electronic mail: puskar.bhattarai@temple.edu

as

$$E_{xc}^{PZ-SIC} = E_{xc}^{approx}[n_{\uparrow}, n_{\downarrow}] - \sum_{\alpha\sigma} \delta_{\alpha\sigma}. \quad (4)$$

Here $\delta_{\alpha\sigma}$ is the SIE of an orbital with quantum numbers α and σ , (where σ is the spin, and α is the orbital quantum number). The orbital density is $n_{\alpha\sigma}(\mathbf{r}) = |\psi_{\alpha\sigma}(\mathbf{r})|^2$, and

$$\delta_{\alpha\sigma} = U[n_{\alpha\sigma}] + E_{xc}^{approx}[n_{\alpha\sigma}, 0]. \quad (5)$$

Use of delocalized KS orbitals for PZ-SIC leads to a size-extensivity problem.⁶ Besides that, they can be highly noded, leading to disastrous results⁷ when applied to the semi-local functionals. Fermi-Löwdin orbitals (FLOs)⁸ correspond to a unitary transformation of KS orbitals and are guaranteed to be localized around Fermi-orbital descriptor (FOD) positions. FLOs are not nodeless but more weakly noded than the KS orbitals, as the overlapping real FLOs must have nodes to establish orthogonality. Complex FLOs (not yet implemented) can achieve orthogonality without having noded orbital densities, but the orbital densities may still be lobed and pose problems for semi-local functionals.^{9,10}

The FLOSIC method^{8,11} has been applied to different density functional approximations (DFAs) to successfully predict various properties of atoms and molecules¹²⁻¹⁸. Applying FLOSIC to the approximate semi-local functional greatly reduces the error for stretched bonds⁷ where SIE is large, but it introduces other errors due to the presence of nodes and lobed structures in the orbital densities, which are not needed by uncorrected DFAs. Besides that, the application of PZ-SIC to the DFAs violates the most common norm of exactness for the uniform electron gas¹⁹, and produces a significant error in the exchange-correlation energy of neutral atoms in the limit of large atomic number Z . PZ-SIC, although it improves the barrier heights of chemical reactions⁷ that include stretched bonds, often worsens equilibrium properties like atomization energies⁷, electron affinities, ionization potential, and bond lengths of molecules¹⁰.

Various scaling functions and methods^{10,20-26} have been introduced to improve the prediction of equilibrium properties like atomization energy. The half-SIC approximation proposed in Ref. 24 does not perform better for both atomization energy and the energy barriers. The scaling proposed in Ref. 20 and Ref. 10 violates the correct asymptotic behavior $\frac{-1}{r}$ of the exchange-correlation potential and produces $\frac{-X_{HO}}{r}$ behavior, where X_{HO} is the scaling factor for the highest occupied orbital. Recently, a new approach called LSIC²⁵ was proposed as an interior scaling of PZ-SIC. It uses an iso-orbital indicator(z_{σ}) as the scaling factor to distinguish one-electron regions from many electron regions. $z_{\sigma} = 0$ is consistent with a region of uniform density and $z_{\sigma} = 1$ is consistent with a one-electron region. z_{σ} is defined by

$$z_{\sigma} = \frac{\tau_{\sigma}^W(\mathbf{r})}{\tau_{\sigma}(\mathbf{r})}, \quad (6)$$

where, $\tau_{\sigma}^W(\mathbf{r})$ is the von Weizsäcker kinetic energy density

$$\tau_{\sigma}^W(\mathbf{r}) = \frac{|\nabla n_{\sigma}|^2}{8n_{\sigma}}. \quad (7)$$

LSIC uses the simplest scaling factor z_{σ} to scale down PZ-SIC and is exact for the uniform gas limit as satisfied by the uncorrected DFAs. LSDA-LSIC, evaluated non-self-consistently on LSDA-SIC FLO densities, improves many calculated properties over PZ-SIC, including covalent binding energies²⁷. However, it fails to recover all of the known asymptotic expansion of E_{xc} for atoms of large atomic number Z .

The exact large- Z asymptotic expansions of E_{xc} ²⁸⁻³¹ is given as,

$$E_{xc} = -A_x Z^{\frac{5}{3}} - A_c Z \ln(Z) + B_{xc} Z + C_x Z^{\frac{2}{3}} + \dots, \quad (8)$$

where LSDA, PBE and almost all other DFAs exactly reproduce A_x and A_c .¹⁹ LSDA-sdSIC and PBE-sdSIC¹⁰ do not recover the coefficient B_{xc} , but, as will be shown below, SCAN-sdSIC recovers the leading coefficients A_x , A_c , and B_{xc} and produces a balanced result. The relevance of the large- Z expansion to valence-electron properties is discussed in Ref. 32. SCAN-sdSIC improves the performance of SCAN where SIEs are important and restores most of the accuracy of SCAN for equilibrium properties, which are severely degraded by SCAN-SIC.¹⁰ SCAN-sdSIC violates the correct asymptotic behavior $\frac{-1}{r}$ of the exchange-correlation potential.

We present here the scaling function $f(z_{\sigma})$ applied to PZ-SIC, in an approximation referred to as LSIC+, that recovers the leading coefficients A_x , A_c , and B_{xc} and also retains the correct asymptotic behavior of the exchange-correlation potential. LSIC+ is exact for the uniform gas limit and produces much less error in E_{xc} of the neutral atoms in the limit of large Z . LSIC+ satisfies at least one more constraint and is expected to work well for both equilibrium and stretched-bond properties.

II. Theory and computational details

The scaled down SIC using LSIC+ is given as

$$E_{xc}^{DFA-LSIC+} = E_{xc}^{DFA} - \sum_{\alpha,\sigma}^{occ} \{U^{LSIC+}[n_{\alpha\sigma}, 0] + E_{xc}^{LSIC+}[n_{\alpha\sigma}, 0]\}, \quad (9)$$

where

$$U^{LSIC+}[n_{\alpha\sigma}, 0] = \frac{1}{2} \int d\mathbf{r} f(z_{\sigma}(\mathbf{r})) n_{\alpha,\sigma}(\mathbf{r}) \int d\mathbf{r}' \frac{n_{\alpha,\sigma}(\mathbf{r}')}{|\mathbf{r} - \mathbf{r}'|}, \quad (10)$$

$$E_{xc}^{LSIC+}[n_{\alpha\sigma}, 0] = \frac{1}{2} \int \mathbf{dr} f(z_{\sigma}(\mathbf{r})) n_{\alpha,\sigma}(\mathbf{r}) \epsilon_{xc}^{DFA}([n_{\alpha,\sigma}, 0], \mathbf{r}). \quad (11)$$

ϵ_{xc}^{DFA} is the exchange-correlation energy density per electron, and $f(z_{\sigma})$ is the scaling factor such that $f(0) = 0$, $f(1) = 1$, i.e., PZ-SIC is scaled in such a way that there is full correction for any one-electron orbital density and no correction for any uniform electron density. For LSIC+, we propose $f(z_{\sigma})$ as

$$f(z_{\sigma}) = \frac{1}{2} + a(z_{\sigma} - \frac{1}{2}) + b(z_{\sigma} - \frac{1}{2})^3 \quad (12)$$

where, $b = 4(1 - a)$. The value of a is chosen to recover the correct coefficient B_{xc} of the large- Z asymptotic expansion of Eq. 8. $a = 0.5$, and $b = 2.0$ make the large- Z asymptotic expansion very close to the exact one. Table I shows the B_{xc} values for LSIC, LSIC+ and SCAN-sdSIC. They are based on calculations performed for four rare gas atoms Neon ($Z = 10$), Argon ($Z = 18$), Krypton ($Z = 36$), and Xenon ($Z = 54$), and extrapolated to $Z \rightarrow \infty$. Here we chose the closed shell atoms to extrapolate and predict the coefficients in order to minimize the effect of shell structure as discussed in Ref. 31. Fig. 1 shows the scaling functions of LSIC and LSIC+ plotted as a function of z_{σ} . LSIC+ produces more correction than LSIC in the region of $0.0 < z_{\sigma} \leq 0.5$ and less correction than LSIC in the region $0.5 \leq z_{\sigma} < 1.0$.

All calculations, including E_{xc} of rare gas atoms, were carried out using a developmental version of the FLOSIC code³³ based on the NRLMOL code.³⁴ We performed spin unpolarized calculations for rare gas atoms and the S22 set.³⁵ All the other calculations are spin polarized. We used the Sadlej basis set³⁶ that includes long-range functions to capture the extended nature of anion orbitals for calculating electron affinity. Optimized all-electron Gaussian basis sets³⁴ were used for all other properties. The FODs were optimized for SIC calculations until the maximum component of force is less than 5×10^{-4} Hartree/Bohr with self-consistent field (SCF) convergence set to 10^{-6} Hartree. Unless otherwise stated, all DFA and DFA-SIC calculations (where DFA = LSDA, PBE, or SCAN) are self-consistent, while all DFA-sdSIC, LSDA-LSIC, and LSDA-LSIC+ calculations are performed as a single, non-SCF step using the optimized DFA-SIC density and Fermi orbital descriptors (FODs).

Full self-consistency requires the complicated implementation of the functional derivative of $f(z_{\sigma})$. Therefore, we used a quasi-SCF version of LSDA-LSIC and LSDA-LSIC+ to obtain the eigenvalue of the highest occupied molecular orbital (HOMO) for calculating the vertical electron affinity. A more detailed description of quasi-self-consistent LSDA-LSIC and LSDA-LSIC+ is presented in Refs. 18, 37, and 38, which argue that the main effect of scaling comes from the scaled potential term rather than the variation of the scaling factor, which would have a minor effect on the results. The quasi-self-consistent version approximates and scales the PZ-SIC

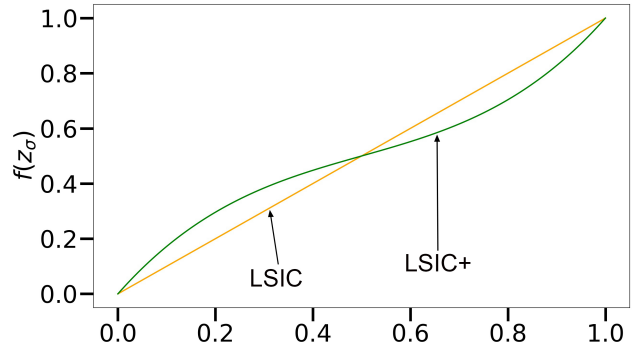


FIG. 1: Scaling functions for LSIC, and LSIC+ as functions of z_{σ} .

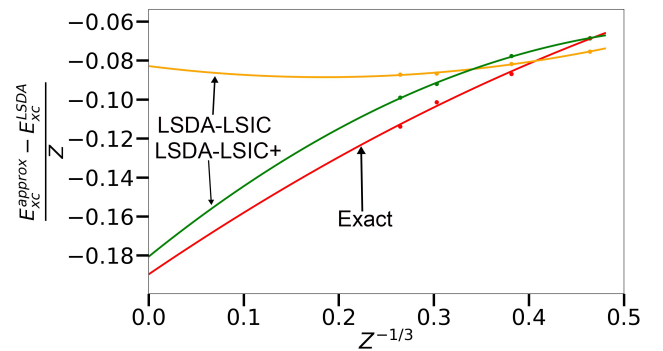


FIG. 2: Extrapolation to $Z^{-1/3} \rightarrow 0$ for the coefficient B_{xc} of the large- Z asymptotic expansion of Eq. 8 for rare gas atoms Neon ($Z = 10$), Argon ($Z = 18$), Krypton ($Z = 36$), and Xenon ($Z = 54$), (in Hartree) against $Z^{-1/3}$. The solid lines represent the extrapolated curves and the solid dots represent the calculated values at $Z = 10, 18, 36$, and 54 .

Note that A_x and A_c are exact in LSDA.

potential as

$$v_{i\sigma}^{interior\ scaled\ SIC} \approx -f(z_{\sigma}(\mathbf{r})) \frac{\delta\{U[n_{i\sigma}] + E_{xc}[n_{i\sigma}, 0]\}}{\delta n_{i\sigma}(\mathbf{r})}. \quad (13)$$

TABLE I: Coefficient of the third term of the large- Z asymptotic expansion of Eq. 8 using the LSDA-LSIC+, LSDA-LSIC, and SCAN-sdSIC methods.

	LSIC+	LSIC	SCAN-sdSIC	Exact
B_{xc}	-0.1806	-0.0828	-0.1755	-0.1868 ³¹

The LSDA E_{xc} values of rare gas atoms calculated with LSDA-SIC density are subtracted from exact^{28,39}, LSDA-LSIC, and LSDA-LSIC+ E_{xc} values, and the result is divided by the atomic number Z . The results thus obtained are plotted against $Z^{-1/3}$ as shown in Fig. 2. The intercept on the y-axis provides the B_{xc} results. The oscillation of the LSDA exchange curve imitates that of the

exact exchange energy curve. Subtracting the LSDA values minimizes the oscillations due to the shell structure.³⁰ Fig. 2 shows that the curve for LSDA-LSIC+ lies very close to the exact curve whereas LSDA-LSIC deviates too much from the exact curve, especially in the higher Z region. We can observe that B_{xc} for LSIC+ is very close to the exact one, as presented in Table I.

Fig. 3 shows the relative percentage error of E_{xc} with LSDA-SIC, LSDA-LSIC, and LSDA-LSIC+ and it demonstrates that LSDA-LSIC and LSDA-LSIC+ respect the norm of the uniform electron gas, since the percentage error for exchange-correlation energy becomes nearly zero in the limit of large Z . These extrapolated errors are slightly different from zero since the extrapolation is performed taking just four points into account. For $Z \rightarrow \infty$, LSDA-SIC has the highest error of 5.46%, LSDA-LSIC has an error of -0.67% and LSDA-LSIC+ has an error of 0.57%. The error of these methods for E_{xc} of rare-gas atoms is shown in table II.

TABLE II: Mean percentage error(MPE) and mean absolute percentage error(MAPE) of E_{xc} for four rare gas atoms Neon($Z = 10$), Argon ($Z = 18$), Krypton ($Z = 36$), and Xenon ($Z = 54$).

	LSIC+	LSIC	LSDA-SIC
MPE	-0.3301	-0.2721	3.6418
MAPE	0.3324	0.5492	3.6418

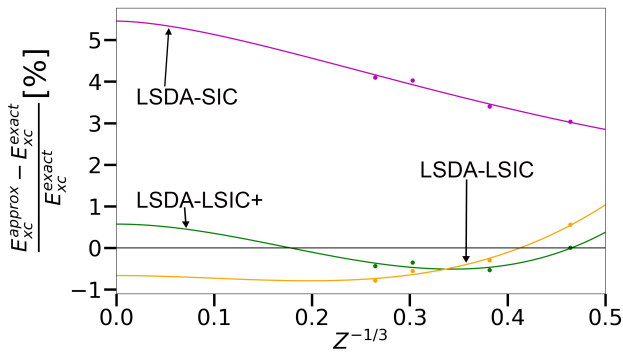


FIG. 3: Extrapolation as in Ref. 19 of percentage error of E_{xc} for rare gas atoms against $Z^{-1/3}$. The solid lines represent the extrapolated curves and the solid dots represent the calculated values at $Z = 10, 18, 36$, and 54 .

III. Results and Discussion

LSIC+ scaling is applied to determine different ground-state properties. We compare several properties of atoms and molecules calculated with LSDA, PBE, and SCAN, with and without SIC, scaled-down SIC(sdSIC)¹⁰, and the interior-scaling methods LSIC and LSIC+ with LSDA. The interior-scaling methods with PBE and especially SCAN do not produce better re-

sults due to gauge inconsistency, which is discussed in detail in Ref. 10. The results for PBE-LSIC and SCAN-LSIC are also presented here for comparison purposes only. We will discuss the results for the total energies of atoms, atomization energies of molecules, barrier heights of chemical reactions, ionization potentials and electron affinities of atoms and molecules, equilibrium bond lengths of molecules, and the interaction energies of a few organic complexes. LSIC and LSIC+ are applied to LSDA, but they produce results close to SCAN results and sometimes even better. Because of the predictive power and success of SCAN^{17,40-45}, the LSDA-LSIC and LSDA-LSIC+ results are primarily compared with SCAN, SCAN-SIC⁴⁶, and SCAN-sdSIC results.

A. Atoms

The mean error (ME), mean absolute error (MAE), and mean absolute percentage error (MAPE) for the total ground state energy of atoms ($Z = 1 - 18$) using different DFAs, their SIC counterparts, and the scaling methods are presented in Table III. Both LSDA-LSIC and LSDA-LSIC+ significantly reduce the error produced by LSDA-SIC. However, LSIC+ generates slightly more error than LSIC. SCAN serves as the best functional in estimating the total ground state energy of atoms. Fig. 4 shows the performances of LSDA-LSIC, LSDA-LSIC+, SCAN, and SCAN-SIC in predicting the total ground state energy of atoms. Both LSDA-LSIC and LSDA-LSIC+ produce an improved result for $Z = 1-10$ and generates the results closer to the reference values⁴⁷. The error for both LSDA-LSIC and LSDA-LSIC+ rises rapidly as we move from $Z = 11$ to $Z = 18$.

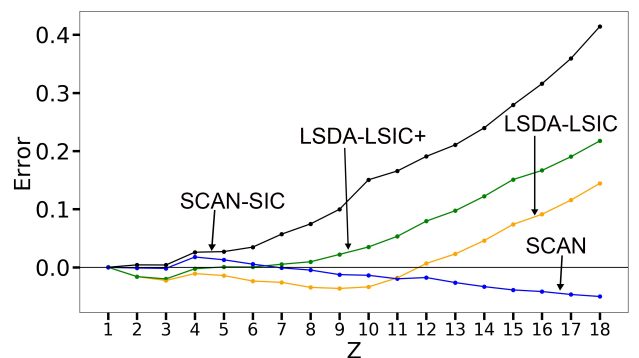


FIG. 4: Error (in Hartree) in the total ground state energy plotted against atomic number Z for atoms from H to Ar.

B. Atomization energy

The atomization energy of a molecule is the energy required to break it into its constituent atoms. Table IV presents the MEs, MAEs and MAPEs of the AE6 set⁴⁸

TABLE III: ME (in Hartree), MAE (in Hartree), and MAPEs for total ground state energies of atoms for atomic number $Z = 1$ to $Z = 18$ for various levels of approximation.

Method	MAE	ME	MAPE
LSDA	0.7261	0.7261	-1.0014
LSDA-SIC	0.3808	-0.3808	-0.2625
LSDA-sdSIC	0.0423	-0.0412	-0.1081
LSDA-LSIC	0.0409	0.0147	-0.0753
LSDA-LSIC+	0.0661	0.0618	-0.0694
PBE	0.0830	0.0830	-0.0995
PBE-SIC	0.1585	0.1585	-0.1091
PBE-sdSIC	0.0710	0.0710	-0.0679
SCAN	0.0192	-0.0152	-0.0217
SCAN-SIC	0.1474	0.1474	-0.0943
SCAN-sdSIC	0.0334	0.0334	-0.0446

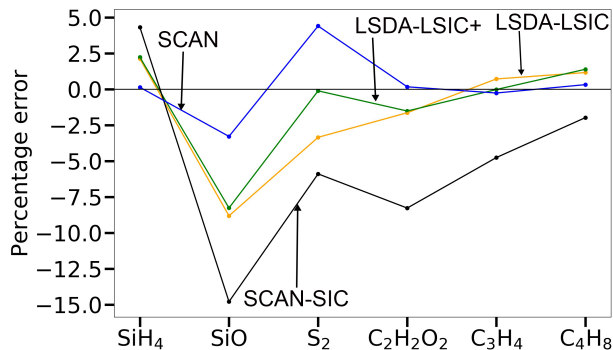
that comprises atomization energies of six representative molecules. Since the reference atomization energies range from 101 kcal/mol to 1149 kcal/mol, it is reasonable to compare percentage error rather than absolute error.

$$\text{Percentage error} = \frac{\text{calculated value} - \text{reference value}}{\text{reference value}} \times 100\% \quad (14)$$

TABLE IV: ME in kcal/mol, MAE in kcal/mol and MAPE for atomization energy of the AE6 set for various levels of approximation.

Approx.	ME	MAE	MAPE
LSDA	75.5	75.5	16.7
LSDA-SIC	53.5	57.8	9.9
LSDA-sdSIC	24.5	25.7	5.6
LSDA-LSIC	-0.9	9.3	3.0
LSDA-LSIC+	-0.4	8.2	2.3
PBE	10.6	13.8	3.8
PBE-SIC	-15.6	17.8	5.5
PBE-sdSIC	6.8	11.7	4.1
SCAN	0.3	3.0	1.4
SCAN-SIC	-24.4	26.1	7.0
SCAN-sdSIC	-3.3	5.7	2.4

LSDA-LSIC+ works better than the LSDA, PBE, their SIC counterparts, and even LSDA-LSIC. The MAPE of LSDA-LSIC+ is close to SCAN and SCAN-sdSIC.¹⁰ Fig. 5 shows the comparison of percentage errors for SCAN, SCAN-SIC, LSDA-LSIC, and LSDA-LSIC+ for the individual molecules. Percentage errors are calculated using Eq. 14. The reference values for calculating the errors for the AE6 set are taken from Ref. 48. SCAN overestimates the atomization energies slightly on average, SCAN-SIC over-corrects and hence underestimates

**FIG. 5:** Percentage errors in atomization energies for individual molecules of the AE6 set by SCAN, SCAN-SIC, LSDA-LSIC, and LSDA-LSIC+.

them. This is because, as we proceed from separated atoms to the molecules they form, the valence orbitals acquire more orbitals with which they overlap and, hence, become more noded. Thus, SIC to SCAN makes the energy of the molecule higher than it would have been if the orbital densities had been nodeless.⁷ SCAN-sdSIC scales down the SCAN-SIC results and yields an accuracy near that of SCAN. The results for the total ground state energy of individual atoms and molecules using LSDA-LSIC, LSDA-LSIC+, SCAN, SCAN-sdSIC, and SCAN-SIC are presented in the supplemental information.

C. Chemical barrier heights

The barrier height of a chemical reaction is the difference between the maximum energy of the transition state and the total energy of the reactants (forward barrier) or the products (reverse barrier). The transition state involves stretched bonds where SIE is expected to be maximal.⁷ LSDA-LSIC and LSDA-LSIC+ both perform almost equally well for the representative set of barrier heights BH6.⁴⁸ The MAE of both the methods is better than that of SCAN-SIC and SCAN-sdSIC. Table V presents the MEs and MAEs of barrier heights for different approximations. The reference values are taken from Ref. 49.

D. Ionization potential

The ionization potential of a system refers to the energy required to remove the most loosely bound electron. The ionization potential can be calculated using either the vertical or the adiabatic method. Here, the adiabatic ionization potential of a system refers to the difference in energy of the neutral system, at its most stable geometry, and of the cationic system, at its stable geometry, whereas vertical ionization potential refers to the difference of the neutral and cationic system in

TABLE V: Mean error (ME) and mean absolute error (MAE) of barrier heights for the BH6 set for various levels of approximation. The values are in kcal/mol.

Approx.	ME	MAE
LSDA	-18.1	18.1
LSDA-SIC	-5.1	5.1
LSDA-sdSIC	-4.1	4.1
LSDA-LSIC	0.6	1.4
LSDA-LSIC+	-0.2	2.1
PBE	-9.6	9.6
PBE-SIC	0	4.6
PBE-sdSIC	-3.7	4.2
SCAN	-7.9	7.9
SCAN-SIC	-1	3
SCAN-sdSIC	-4.6	4.6

the stable geometry of the neutral. This means that, in the vertical method, we assume that the geometry of the system remains unchanged even after the removal of an electron. In the ΔSCF method, the ionization potential is obtained as the difference between the total ground state energy of the neutral and the cationic system. The vertical ionization potential can also be accessed by using Janak’s theorem,⁵⁰ i.e., the derivative of total energy with respect to orbital occupation is equal to the eigenvalue of that orbital ($\frac{\partial E}{\partial f_i} = \epsilon_i$), independent of the detailed form of the exchange-correlation functional. This implies that the exact vertical ionization potential is simply the negative of the exact KS HOMO eigenvalue of the neutral system.^{51,52} Table VI shows the adiabatic ionization potential of the G2-1 set.^{53,54} For the adiabatic ionization potential with the ΔSCF method, LSDA-LSIC+ improves over LSDA-LSIC and is almost competitive with SCAN and SCAN-sdSIC. The vertical ionization potential result of the same test set accessed using Janak’s theorem is presented in Ref. 38. For a set of intermediate-sized organic molecules³⁸, the error in the highest-occupied orbital energy is 0.83 eV for LSDA-LSIC+ and 1.13 eV for LSDA-LSIC.

E. Electron affinity

The electron affinity of a neutral system is defined as the change in energy when an extra electron is added in its isolated gaseous phase. Tables VII and VIII show the MEs and MAEs of the electron affinities of the G2-1 set^{53,54} using vertical and adiabatic methods, respectively. The adiabatic electron affinity assumes that the geometry of the system is relaxed after the addition of an electron. In the vertical method, we assume that the geometry of the system remains unchanged even after adding an extra electron. In the ΔSCF method, electron affinity is obtained as the difference between the total ground state energy of the neutral and anionic sys-

TABLE VI: Mean error (ME), and mean absolute error (MAE) of the adiabatic ionization potential of the G2-1 set using the ΔSCF method for various levels of approximation. The reference values are taken from Ref. 55. The values are in kcal/mol.

Method	ME	MAE
LSDA	2.7	6.2
LSDA-SIC	7.0	10.3
LSDA-sdSIC	3.6	7.8
LSDA-LSIC	2.7	7.1
LSDA-LSIC+	1.4	6.4
PBE	-0.8	4.8
PBE-SIC	-4.7	10.6
PBE-sdSIC	0.8	6.8
SCAN	-0.9	5.8
SCAN-SIC	-5.4	8.3
SCAN-sdSIC	-1.2	5.5

tems. For an exact functional, the negative of the eigenvalue of the HOMO of an anionic system yields the vertical electron affinity.^{51,52} We have accessed the vertical electron affinity of the G2-1 set with this method. Semi-local DFAs fail to capture an extra electron in the anionic system. Hence, LSDA, PBE, and SCAN results presented here are single step non-SCF calculations with the SCAN-SIC density. LSIC and LSIC+ have equal MAEs for the adiabatic electron affinity and perform better than SCAN and SCAN-sdSIC. However, LSIC+ seems to be superior to LSIC for the vertical electron affinity of the G2-1 set. As single step non-SCF calculations do not produce eigenvalues, the quasi-SCF versions of LSIC and LSIC+ are used to calculate vertical electron affinity.

TABLE VII: MEs and MAEs of the vertical electron affinity of the G2-1 set, calculated by using the eigenvalue of the HOMO. All values are in kcal/mol.

Method	ME	MAE
LSDA	-75.0	75.0
LSDA-SIC	30.2	30.2
LSDA-LSIC	6.5	8.9
LSDA-LSIC+	-1.4	6.3

F. Equilibrium bond length

Table IX shows the MEs and MAEs of the equilibrium bondlengths of a benchmark set of 11 diatomic molecules²⁰, evaluated by finding the minimum of the quadratic fit of the total energy over varying bond length. SCAN performs much better than any other functional. LSIC and LSIC+ values lie in between SCAN and SCAN-SIC, with LSIC having a slightly better result than the LSIC+ and closer to SCAN-sdSIC results.

TABLE VIII: MEs and MAEs of the adiabatic electron affinity of the G2-1 set, calculated by the ΔSCF method. All values are in kcal/mol. The reference values are taken from Ref. 53.

Method	ME	MAE
LSDA	5.7	5.9
LSDA-SIC	-1.4	5.6
LSDA-sdSIC	-0.3	3.4
LSDA-LSIC	1.5	3.2
LSDA-LSIC+	-0.2	3.2
PBE	1.3	2.0
PBE-SIC	-13.2	13.4
PBE-sdSIC	-4.5	4.6
SCAN	-0.3	4.1
SCAN-SIC	-9.0	9.4
SCAN-sdSIC	-2.8	5.2

TABLE IX: MEs and MAEs of the equilibrium bond lengths of a benchmark set²⁰ of 11 diatomic molecules (in angstrom). Results other than those for LSIC+ are the same as in Table VIII of Ref. 10, where the large improvement due to interior-scaling of the SIC was first found.

Method	ME	MAE
LSDA	0.0076	0.0110
LSDA-SIC	-0.0317	0.0392
LSDA-sdSIC	-0.0085	0.0189
LSDA-LSIC	-0.0015	0.0129
LSDA-LSIC+	-0.0024	0.0147
PBE	0.0123	0.0123
PBE-SIC	-0.0134	0.0257
PBE-sdSIC	-0.0019	0.0132
SCAN	0.0039	0.0057
SCAN-SIC	-0.0190	0.0197
SCAN-sdSIC	-0.0110	0.0110

G. Dissociation energy of noncovalently bonded complexes

The S22 dataset³⁵ consists of the dissociation energies of complexes built up from pairs of small to large, mostly organic molecules, at reference geometries. These complexes are divided into three categories: hydrogen bonded complexes, complexes with predominant dispersion interactions, and mixed complexes (with both kinds of bonds). We tested the performance of different approximations on this dataset. Table X presents the MEs and MAEs in kcal/mol for these functionals. All of our calculations in Table X are spin unpolarized and self-consistent, with the exception of LSDA-LSIC and LSDA-LSIC+ (evaluated on LSDA-SIC total and localized orbital densities) and SCAN-sdSIC (evaluated on SCAN-SIC total and lo-

calized orbital densities). While the other functionals perform reasonably well, both interior-scaled functionals, LSDA-LSIC and LSDA-LSIC+, consistently underestimate the binding of the complexes, in several cases predicting them to be unbound. Detailed results for the individual molecules are presented in the supplemental information. Until we can implement LSDA-LSIC and LSDA-LSIC+ self-consistently, we cannot say whether their failures for weak bonds might be corrected by full self-consistency. All we can say is that the LSDA-SIC and SCAN-SIC densities and FLO densities on which they are evaluated are not by themselves wrong, since the LSDA-SIC and SCAN-SIC S22 binding energies are reasonable.

It might be surprising that the original PZ SIC (labelled SIC in Table X) is not worse than it is for the S22 set, since the self-interaction corrections from the valence orbitals are large in comparison with the weak binding energies of the S22 complexes. The explanation for this lies in the chemical interpretation of the FLOs as covalent double bonds, covalent single bonds, lone pairs, and core orbitals. These orbitals are often changed only modestly when weak bonds are broken. Thus most of the self-interaction correction from the valence electrons cancels out of the binding energies of the complexes. The cancellation is even more perfect when the weak bonds are not all broken but are simply re-arranged, as in the structural energy differences among the water hexamers¹⁷. An exception⁵⁶ to the partial cancellation upon weak-bond breaking is the hydrogen bond in $H_3O^+(H_2O)$, which is strong enough to induce a transition of electrons between covalent-bond orbitals and lone-pair orbitals.

The cancellation in PZ SIC discussed in the previous paragraph can be lost in LSDA-LSIC (evaluated on LSDA-SIC densities and orbitals). The FLO densities are what they were in LSDA-SIC, but their contributions to the self-interaction correction are now scaled down, and the scaling can be stronger in the overlap region than in the corresponding regions of the same monomer or isolated molecule. This arises because of a reduction in the scaling parameters z_σ and $f(z_\sigma)$ in the region where the charge from the two components in a given complex overlaps.

In $(H_2O)_2$, for example, the sum of the orbital self-interaction corrections to the total energy differs by only 0.2 mHa from the sum of the corresponding SIC orbital energies in the two isolated molecules. In the LSIC calculation, however, this difference is 10.0 mHa (about 6 kcal/mol). This difference can be traced to contributions from FLOs corresponding to the O lone-pair orbital and the O-H bond orbital that are located in the overlap region between the two water molecules. Fig. 6 shows the comparison of the total electron density n and the scaling factor z_σ of the water dimer along the bond axis of O-H in the overlapping region and the corresponding non-overlapping region. The plot omits the very large density near the O atom nucleus. It can be seen that the value of z_σ as well as n remains similar up to the position

of the H atom at about 0.96 Å. The density remains almost equal until about 1.5 Å but z_σ differs significantly. After about 1.5 Å, the density in the overlapping region increases because of the presence of the lone pair electron of another water molecule. The scaling factor z_σ ($f(z_\sigma)$ for LSIC+) is seen to be smaller in the overlap region than at corresponding locations outside the overlap region or in the isolated molecules. Because of this, the LSIC energies for these orbitals are relatively smaller in magnitude than the LSIC energies for the corresponding orbitals in the isolated molecules, resulting in the energy difference noted above. Because the LSDA-SIC and LSDA-LSIC orbital energies are negative, and the energy densities that get scaled down are primarily negative, the implication is that the complex is relatively less stable in LSDA-LSIC than in LSDA-SIC. Similar effects are found for other complexes we have analyzed.

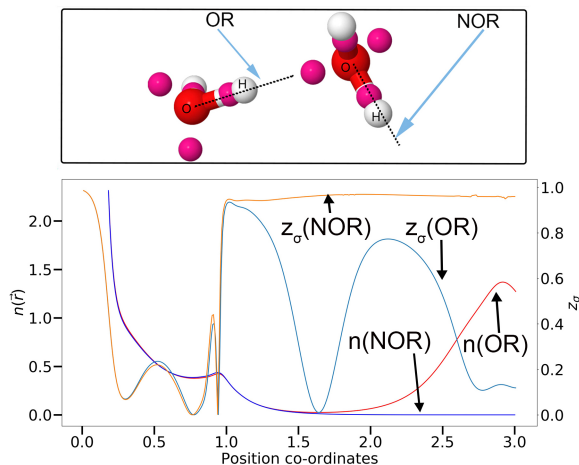


FIG. 6: Comparison of the total electron density n and the scaling factor z_σ in the overlapping region (OR) and a corresponding non-overlapping region (NOR) of the water dimer. The position of the O atom is at the origin for each curve. In the inset is a diagram that shows the positions of the O (red) and H (white) atoms, as well as the FOD positions (pink). The scaling factor and the total electron density are plotted along the dotted lines shown on the inset. The position co-ordinates are in Å and the total electron densities are in atomic units.

Why is the scaling factor smaller in the overlap region? z_σ is close to one in one-electron regions of the charge density. Far from the center of an isolated molecule, the density tends to be dominated by contributions from a single orbital and z_σ is correspondingly close to one. In the overlapping charge region of the molecular complex, however, the density decreases to a minimum moving away from one molecule and then increases again on nearing the second molecule. Since z_σ depends on the gradient of the density (see Eq. 7), the scaling factor must be close to zero near this minimum.

Performing self-consistent LSDA-LSIC and LSDA-LSIC+ calculations could improve the results for the S22

interaction energies. Shifting the electron density in the overlap region of the complexes slightly could have a significant impact on the scaling parameters z_σ and $f(z_\sigma)$ without changing other quantities that affect the total energy. Alternatively, employing LSDA-LSIC and LSDA-LSIC+ -type approaches with scaling functions based on improved iso-orbital indicators α^{57} or β^{58} could also improve the results for the interaction energies. Unlike z_σ , these indicators can distinguish densities associated with weak (i.e., van der Waals or hydrogen) bonds from slowly-varying densities.

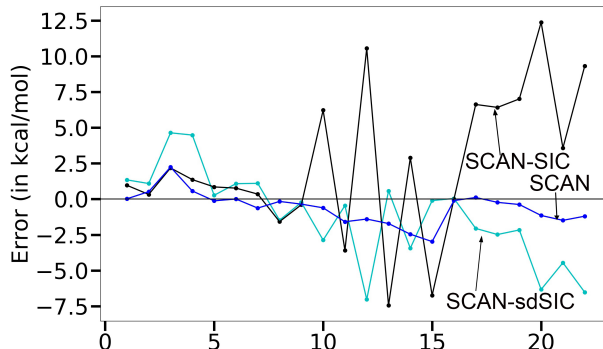


FIG. 7: Individual errors (in kcal/mol) for the dissociation energy of complexes of the S22 dataset

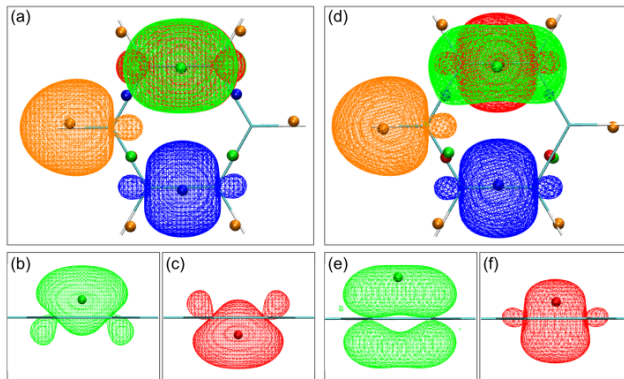


FIG. 8: FLO densities of the benzene molecule obtained using two FOD arrangements. The *sym* arrangement yields the FLOs in panel (a) (top view) and (b) and (c) (side views). The *asym* arrangement gives the FLOs in panel (d), (e) and (f). FLOs corresponding to C-H bonds (orange), C-C single bonds (blue), and C-C double bonds (red and green) are shown. Isosurface values of $0.001 e/\text{\AA}^3$ were used to make all FLO images. FODs corresponding to each FLO type are shown by small spheres of the corresponding color.

In the side views, only the double bond FLOs are shown along with the corresponding FOD positions.

Another conclusion from Table X and Ref. 10 is that SCAN-sdSIC, evaluated on SCAN-SIC densities and FLOs, is almost uniformly more accurate than SCAN-LSIC or SCAN-LSIC+ evaluated on LSDA-SIC densities and FLOs for equilibrium properties of molecules, and

TABLE X: The dissociation energy of weakly bound complexes in the S22 dataset. All values are in kcal/mol. The calculations are spin-restricted. The reference values are taken from Ref. 59. A negative ME indicates that an approximation underestimates the binding, on average.

	ME	MAE
LSDA	2.16	2.18
LSDA-SIC	1.41	2.98
LSDA-LSIC	-8.95	9.77
LSDA-LSIC+	-7.00	7.42
PBE	-2.56	2.58
PBE-SIC	-2.64	2.97
SCAN	-0.60	0.91
SCAN-SIC	2.37	4.16
SCAN-sdSIC	-1.14	2.46

especially so for the weakly-bound complexes. Figure 7 shows the individual errors in the dissociation energy of the complexes in the S22 database by SCAN, SCAN-SIC, and SCAN-sdSIC. SCAN-sdSIC overestimates and makes slightly more error than both SCAN and SCAN-SIC for hydrogen-bonded complexes (complexes 1-7). SCAN-sdSIC restores the capacity of SCAN to capture the short and intermediate range van der Waals interactions involved in the complexes with predominant dispersion contribution (complexes 8-15) and the mixed complexes (complexes 16-22) which are somewhat degraded from SCAN to SCAN-SIC. Hence, SCAN-sdSIC might be a better option to scale down the PZ-SIC and predict the properties of weakly bonded systems.

H. Do the FLOs have a consistent chemical interpretation?

The FLOs are often interpreted chemically as covalent double bonds, covalent single bonds, lone pairs, etc. But this interpretation is only useful if it can be made consistently. The benzene molecule is a challenging example in this context. There are two distinct solutions for the spin unpolarized benzene monomer in LSDA-SIC. In one (*sym*), the FODs are as shown in Fig. 8: for the C-C bonds around the ring, a single FOD at the center of one bond alternates with a pair of FODs that are symmetrically placed above and below the bond center of the next, nominally representing single (C-C) and double (C=C) bonds, respectively. The single bond FOD gives rise to the FLO density depicted in blue in Fig. 8, while the double bond FODs give rise to a pair of symmetric FLOs, one above the plane of the molecule and the below, its mirror image, below it (Fig. 8 (b) and (c)). In the other solution (*asym*), the double bond FODs both lie on the same side of the molecular plane. In this case, the single-bond FLO is essentially unchanged from the *sym* solution, but

the double bond FLOs change shape dramatically to the red and green FLO densities shown in Fig. 8 (e) and (f).

(Note that it is the FODs, and not the FLO densities, that can be strongly asymmetric around the plane of the molecule.) The red FLO is very similar to the single bond FLO and can be thought of as a bonding combination of sp^2 hybrid orbitals. The green FLO can be thought of as a bonding combination of p_z orbitals and has a node in the molecular plane. In the *sym* solution, the symmetric double bond FLOs each have an SIC energy of -0.016 Ha. In the *asym* solution, the red and green FLOs have SIC energies of -0.048 and +0.023 Ha, respectively. Despite this, the total energy of the *asym* solution is only 1.4 mHa (0.9 kcal/mol) lower in energy than the *sym* solution in LSDA-SIC. This remarkable near degeneracy is broken in LSDA-LSIC, where the ordering switches and the *sym* solution is lower by 23.2 mHa (14.6 kcal/mol). In the benzene-containing complexes, we only found *asym*-type LSDA-SIC solutions, despite using *sym*-type starting points for the FODs. The *asym* and *sym* solutions are also nearly degenerate in PBE-SIC.

There is also a third nearly degenerate solution for the benzene monomer if spin polarized densities are considered. This solution (*Linnett*) has been discussed elsewhere⁶⁰ and can be linked to the Linnett double quartet bonding theory,^{61,62} a spin-polarized generalization of Lewis theory. In this case, *sym*-type FOD arrangements in the up and down spin channels are shifted by one bond around the ring, so that each bond has a single FOD of one spin at the bond center and two FODs of the opposite spin placed symmetrically above and below the center. The FLOs for the *Linnett* solution are very similar to the *sym* FLOs shown in Fig. 8. The total energy of the *Linnett* solution in LSDA-SIC is slightly lower (1.3 mHa = 0.8 kcal/mol) than that of the *asym* solution. For the parallel-displaced benzene dimer (S22 complex 11), we find that the *Linnett* solution for the dimer is also slightly lower than the *asym* dimer, so that the calculated dissociation energies are nearly identical, 1.6 kcal/mol and 1.1 kcal/mol for *Linnett* and *asym* respectively. The data in Table X reflect spin unpolarized calculations only. We do not expect that significant differences would arise if spin-polarized *Linnett* arrangements were used for all complexes containing benzene.

The way to find the localized orbitals suggested by Perdew and Zunger 1981, and universally applied since then, is to choose the unitary transformation of the canonical or generalized Kohn-Sham orbitals that minimizes the self-interaction-corrected total energy. But that approach is inconsistent with the chemical interpretation of the FLOs. To preserve a consistent chemical interpretation, we need a new way to select the optimum unitary transformation, for example, by minimizing a measure of the inhomogeneity of the FLO densities. Such a measure should penalize all strongly noded or lobed orbital densities such as the green ones in Fig. 8 (d) and (e).

The nuclear geometry used here for benzene is unchanged under 60-degree rotations around a central axis. There must be an exact ground-state electron density that preserves this symmetry.⁶³ The single-determinant auxiliary wave functions that we have calculated break this symmetry. In either the spin unpolarized *sym/asym* or the *Linnett* scheme, there are two degenerate Slater determinants with different densities (*sym/asym*) or spin densities (*Linnett*), the density or spin density of one determinant transforming into that of the other under a 60-degree rotation. A possible physical interpretation⁶³ is that there are low-frequency fluctuations of the density and spin-density that anti-correlate on alternate bonds around the benzene ring.

IV. Summary and conclusions

We introduced LSIC+ that takes the iso-orbital indicator z_σ as its argument for interior scaling of Perdew-Zunger self-interaction correction. LSIC+ is applied with LSDA only and not with GGAs and meta-GGAs to avoid gauge-inconsistency. LSIC+ is an improved version of LSIC²⁵ that satisfies one more constraint from the large- Z asymptotic expansion of exchange-correlation energy, in addition to restoring the correct uniform density limit of the exchange energy violated by PZ-SIC. The relevance of the uniform-density and large- Z limits to valence-electron properties was explained in Ref. 32. LSIC+ retains the full PZ-SIC in the region of one-electron density, giving no correction for uniform electron density, and a scaled correction in the region in between. Hence, LSDA-LSIC+ works well for both stretched bond cases and equilibrium properties that do not involve weak bonds. We present here the results of LSDA-LSIC+ for ground state energies of atoms from $Z=1-18$, atomization energies of the AE6 set, chemical barrier heights of the BH6 set, ionization potentials of the G2-1 set, electron affinities of the G2-1 set, equilibrium bond lengths, and interaction energies of the S22 set of weakly-bonded complexes, and compare with LSDA-LSIC and other SIC-corrected and uncorrected DFAs. LSDA-LSIC+ performs better than LSDA-LSIC for most of the properties and comparably for a few. LSDA-LSIC+ is even better than SCAN or SCAN-SIC for a few properties such as total ground state energy of atoms and electron affinity. LSIC+ satisfies one more constraint than LSIC and produces better results than LSIC, which shows the significance of constraint satisfaction in the construction of functionals. The better performance of SCAN-sdSIC can also be attributed to the recovery of higher-order coefficients in the asymptotic expansion of exchange-correlation energy for atoms of large Z . However, since LSIC and LSIC+ employ functions of z_σ , they cannot recognize⁶⁴ weaker bonds and (at least when evaluated on LSDA-SIC total and localized orbital densities) produce poor results for the van der Waals or hydrogen-bond binding energies.

Surprisingly, the Fermi-Löwdin orbitals that describe multiple covalent bonds are not unique. Two different

versions give nearly degenerate LSDA-SIC energies in benzene-like systems, though not in LSDA-LSIC. A more physical way to determine the Fermi orbital descriptors is needed to give a single, consistent picture of these FLOs.

Unlike LSIC and LSIC+, SCAN-sdSIC is applied to the more accurate SCAN functional, which is already much better than LSDA and hence improves its predictive power. It provides good results for several ground state properties discussed here, including the dissociation energy of weakly bonded systems. The SCAN-sdSIC, if scaled down by functions of improved iso-orbital indicators α or β , may further improve the results.²⁶ However, since SCAN-sdSIC provides an incorrect asymptote $-\frac{X_{HO}}{r}$ for the exchange-correlation potential, it does not guarantee a good description of charge transfer. The optimal SIC that remains to be developed might be PZ SIC evaluated on complex⁶⁵ Fermi-Löwdin orbitals⁶⁶ (with nodeless^{7,65} orbital densities) and with Fermi orbital descriptors chosen to minimize a measure of the inhomogeneity of the orbital densities.

Acknowledgments

This work was supported by the U.S. Department of Energy, Office of Science, Office of Basic Energy Sciences, as part of the Computational Chemical Sciences Program under Award No. DE-SC0018331. The work of P.B. and KW. was supported by the U.S. National Science Foundation under Grant No. DMR-1939528. This research includes calculations carried out on HPC resources supported in part by the National Science Foundation through major research instrumentation grant number 1625061 and by the US Army Research Laboratory under contract number W911NF-16-2-0189. A few calculations were carried out on the EFRC cluster supported by the Department of Energy (DOE), Office of Science (OS), Basic Energy Sciences (BES) through Grant No. DE-SC0012575 to the Energy Frontier Research Center: Center for Complex Materials from First Principles. The plots are generated by MATPLOTLIB.⁶⁷

V. Supplemental material

The detailed results of ground state energy of atoms ($Z=1-18$), the energy of individual atoms, and molecules of the AE6 set and the S22 dataset can be accessed through supplementary material. Other data in detail that support the findings of the study are available from the corresponding author upon reasonable request.

¹W. Kohn and L. J. Sham, *Physical Review* **140**, A1133 (1965).

²J. P. Perdew and K. Schmidt, *AIP Conference Proceedings* **577**, 1 (2001).

³J. Sun, A. Ruzsinszky, and J. P. Perdew, *Physical Review Letters* **115**, 036402 (2015).

- ⁴J. P. Perdew, K. Burke, and M. Ernzerhof, *Physical Review Letters* **77**, 3865 (1996).
- ⁵J. P. Perdew and Y. Wang, *Physical Review B* **45**, 13244 (1992).
- ⁶J. P. Perdew and A. Zunger, *Physical Review B* **23**, 5048 (1981).
- ⁷C. Shahi, P. Bhattarai, K. Wagle, B. Santra, S. Schwalbe, T. Hahn, J. Kortus, K. A. Jackson, J. E. Peralta, K. Treppe, S. Lehtola, N. K. Nepal, H. Myneni, B. Neupane, S. Adhikari, A. Ruzsinszky, Y. Yamamoto, T. Baruah, R. R. Zope, and J. P. Perdew, *The Journal of Chemical Physics* **150**, 174102 (2019).
- ⁸M. R. Pederson, A. Ruzsinszky, and J. P. Perdew, *The Journal of Chemical Physics* **140**, 121103 (2014).
- ⁹D. Hofmann, S. Klüpfel, P. Klüpfel, and S. Kümmel, *Physical Review A* **85**, 062514 (2012).
- ¹⁰P. Bhattarai, K. Wagle, C. Shahi, Y. Yamamoto, S. Romero, B. Santra, R. R. Zope, J. E. Peralta, K. A. Jackson, and J. P. Perdew, *The Journal of Chemical Physics* **152**, 214109 (2020).
- ¹¹Z.-h. Yang, M. R. Pederson, and J. P. Perdew, *Physical Review A* **95**, 052505 (2017).
- ¹²M. R. Pederson, *The Journal of Chemical Physics* **142**, 064112 (2015).
- ¹³K. Sharkas, L. Li, K. Treppe, K. P. Withanage, R. P. Joshi, R. R. Zope, T. Baruah, J. K. Johnson, K. A. Jackson, and J. E. Peralta, *The Journal of Physical Chemistry A* **122**, 9307 (2018).
- ¹⁴R. P. Joshi, K. Treppe, K. P. Withanage, K. Sharkas, Y. Yamamoto, L. Basurto, R. R. Zope, T. Baruah, K. A. Jackson, and J. E. Peralta, *The Journal of Chemical Physics* **149**, 164101 (2018).
- ¹⁵K. P. K. Withanage, S. Akter, C. Shahi, R. P. Joshi, C. Diaz, Y. Yamamoto, R. Zope, T. Baruah, J. P. Perdew, J. E. Peralta, and K. A. Jackson, *Physical Review A* **100**, 012505 (2019).
- ¹⁶A. I. Johnson, K. P. Withanage, K. Sharkas, Y. Yamamoto, T. Baruah, R. R. Zope, J. E. Peralta, and K. A. Jackson, *The Journal of Chemical Physics* **151**, 174106 (2019).
- ¹⁷K. Sharkas, K. Wagle, B. Santra, S. Akter, R. R. Zope, T. Baruah, K. A. Jackson, J. P. Perdew, and J. E. Peralta, *Proceedings of the National Academy of Sciences* **117**, 11283 (2020).
- ¹⁸K. P. K. Withanage, P. Bhattarai, J. E. Peralta, R. R. Zope, T. Baruah, J. P. Perdew, and K. A. Jackson, accepted in *The Journal of Chemical Physics*.
- ¹⁹B. Santra and J. P. Perdew, *The Journal of Chemical Physics* **150**, 174106 (2019).
- ²⁰O. A. Vydrov, G. E. Scuseria, J. P. Perdew, A. Ruzsinszky, and G. I. Csonka, *The Journal of Chemical Physics* **124**, 094108 (2006).
- ²¹O. A. Vydrov and G. E. Scuseria, *The Journal of Chemical Physics* **124**, 191101 (2006).
- ²²A. Ruzsinszky, J. P. Perdew, G. I. Csonka, O. A. Vydrov, and G. E. Scuseria, *The Journal of Chemical Physics* **126**, 104102 (2007).
- ²³A. Ruzsinszky, J. P. Perdew, G. I. Csonka, O. A. Vydrov, and G. E. Scuseria, *The Journal of Chemical Physics* **125**, 194112 (2006).
- ²⁴S. Klüpfel, P. Klüpfel, and H. Jónsson, *The Journal of Chemical Physics* **137**, 124102 (2012).
- ²⁵R. R. Zope, Y. Yamamoto, C. M. Diaz, T. Baruah, J. E. Peralta, K. A. Jackson, B. Santra, and J. P. Perdew, *The Journal of Chemical Physics* **151**, 214108 (2019).
- ²⁶Y. Yamamoto, S. Romero, T. Baruah, and R. R. Zope, *The Journal of Chemical Physics* **152**, 174112 (2020).
- ²⁷L. Li, K. Treppe, K. A. Jackson, and J. K. Johnson, *The Journal of Physical Chemistry A* **124**, 8223 (2020).
- ²⁸K. Burke, A. Cancio, T. Gould, and S. Pittalis, *The Journal of Chemical Physics* **145**, 054112 (2016).
- ²⁹J. Schwinger, *Physical Review A* **24**, 2353 (1981).
- ³⁰P. Elliott and K. Burke, *Canadian Journal of Chemistry* **87**, 1485 (2009).
- ³¹A. Cancio, G. P. Chen, B. T. Krull, and K. Burke, *The Journal of Chemical Physics* **149**, 084116 (2018).
- ³²A. D. Kaplan, B. Santra, P. Bhattarai, K. Wagle, S. T. u. R. Chowdhury, P. Bhetwal, J. Yu, H. Tang, K. Burke, M. Levy, and J. P. Perdew, *The Journal of Chemical Physics* **153**, 074114 (2020).
- ³³FLOSIC 0.2 developed by R. R. Zope, T. Baruah, J. E. Peralta, and K. A. Jackson, .
- ³⁴D. Porezag and M. R. Pederson, *Physical Review A* **60**, 2840 (1999).
- ³⁵P. Jurečka, J. Šponer, J. Černý, and P. Hobza, *Physical Chemistry Chemical Physics* **8**, 1985 (2006).
- ³⁶A. J. Sadlej, *Theoretica Chimica Acta* **81**, 45 (1991).
- ³⁷S. Akter, Y. Yamamoto, C. M. Diaz, K. A. Jackson, R. R. Zope, and T. Baruah, *The Journal of Chemical Physics* **153**, 164304 (2020).
- ³⁸S. Adhikari, B. Santra, S. Ruan, P. Bhattarai, N. K. Nepal, K. A. Jackson, and A. Ruzsinszky, *The Journal of Chemical Physics* **153**, 184303 (2020).
- ³⁹A. D. Becke, *Physical Review A* **38**, 3098 (1988).
- ⁴⁰E. B. Isaacs and C. Wolverton, *Physical Review Materials* **2**, 063801 (2018).
- ⁴¹J. H. Yang, D. A. Kitchaev, and G. Ceder, *Physical Review B* **100**, 035132 (2019).
- ⁴²Y. Zhang, J. W. Furness, B. Xiao, and J. Sun, *The Journal of Chemical Physics* **150**, 014105 (2019).
- ⁴³N. K. Nepal, L. Yu, Q. Yan, and A. Ruzsinszky, *Physical Review Materials* **3**, 073601 (2019).
- ⁴⁴S. Adhikari, H. Tang, B. Neupane, A. Ruzsinszky, and G. I. Csonka, *Physical Review Materials* **4**, 025005 (2020).
- ⁴⁵N. K. Nepal, A. Ruzsinszky, and J. E. Bates, *Physical Review B* **97**, 115140 (2018).
- ⁴⁶Y. Yamamoto, C. M. Diaz, L. Basurto, K. A. Jackson, T. Baruah, and R. R. Zope, *The Journal of Chemical Physics* **151**, 154105 (2019).
- ⁴⁷S. J. Chakravorty, S. R. Gwaltney, E. R. Davidson, F. A. Parpia, and C. F. Fischer, *Physical Review A* **47**, 3649 (1993).
- ⁴⁸B. J. Lynch and D. G. Truhlar, *The Journal of Physical Chemistry A* **107**, 8996 (2003).
- ⁴⁹L. Goerigk, A. Hansen, C. Bauer, S. Ehrlich, A. Najibi, and S. Grimme, *Physical Chemistry Chemical Physics* **19**, 32184 (2017).
- ⁵⁰J. Janak, *Physical Review B* **18**, 7165 (1978).
- ⁵¹J. P. Perdew and M. Levy, *Physical Review B* **56**, 16021 (1997).
- ⁵²J. P. Perdew, R. G. Parr, M. Levy, and J. L. Balduz, *Physical Review Letters* **49**, 1691 (1982).
- ⁵³L. A. Curtiss, K. Raghavachari, G. W. Trucks, and J. A. Pople, *The Journal of Chemical Physics* **94**, 7221 (1991).
- ⁵⁴L. A. Curtiss, K. Raghavachari, P. C. Redfern, and J. A. Pople, *The Journal of Chemical Physics* **106**, 1063 (1997).
- ⁵⁵L. A. Curtiss, P. C. Redfern, and K. Raghavachari, *The Journal of Chemical Physics* **126**, 084108 (2007).
- ⁵⁶K. Wagle, B. Santra, P. Bhattarai, C. Shahi, K. A. Jackson, and J. P. Perdew, in preparation.
- ⁵⁷J. Tao, J. P. Perdew, V. N. Staroverov, and G. E. Scuseria, *Physical Review Letters* **91**, 146401 (2003).
- ⁵⁸J. W. Furness and J. Sun, *Physical Review B* **99**, 041119 (2019).
- ⁵⁹M. S. Marshall, L. A. Burns, and C. D. Sherrill, *The Journal of Chemical Physics* **135**, 194102 (2011).
- ⁶⁰S. Schwalbe, K. Treppe, L. Fiedler, A. I. Johnson, J. Kraus, T. Hahn, J. E. Peralta, K. A. Jackson, and J. Kortus, *Journal of Computational Chemistry* **40**, 2843 (2019).
- ⁶¹J. Linnett, *Nature* **187**, 859 (1960).
- ⁶²J. Linnett, *Journal of the American Chemical Society* **83**, 2641 (1961).
- ⁶³J. P. Perdew, A. Ruzsinszky, N. K. Nepal, and A. D. Kaplan, *Proceedings of the National Academy of Sciences* (to appear).
- ⁶⁴J. Sun, B. Xiao, Y. Fang, R. Haunschild, P. Hao, A. Ruzsinszky, G. I. Csonka, G. E. Scuseria, and J. P. Perdew, *Physical Review Letters* **111**, 106401 (2013).
- ⁶⁵S. Klüpfel, P. Klüpfel, and H. Jónsson, *Physical Review A* **84**, 050501 (2011).

⁶⁶M.R. Pederson, Carlos M. Diaz, work in progress.

⁶⁷J. D. Hunter, *Computing in Science Engineering* **9**, 90 (2007).